Nuclear Instruments and Methods in Physics Research B 412 (2017) 1–10

Contents lists available at ScienceDirect

Nuclear Instruments and Methods in Physics Research B

journal homepage: www.elsevier.com/locate/nimb

Multiple ion beam irradiation for the study of radiation damage in materials

Stephen Taller [a,*], David Woodley [a], Elizabeth Getto [b], Anthony M. Monterrosa [a], Zhijie Jiao [a], Ovidiu Toader [a], Fabian Naab [a], Thomas Kubley [a], Shyam Dwaraknath [c], Gary S. Was [a]

[a] University of Michigan, Ann Arbor, MI 48109, USA
[b] United States Naval Academy, Annapolis, MD 21402, USA
[c] Lawrence Berkeley National Laboratory, Berkeley, CA 94720, USA

ARTICLE INFO

Article history:
Received 8 June 2017
Received in revised form 28 August 2017
Accepted 28 August 2017

Keywords:
Ion irradiation
Radiation damage
Reactors

ABSTRACT

The effects of transmutation produced helium and hydrogen must be included in ion irradiation experiments to emulate the microstructure of reactor irradiated materials. Descriptions of the criteria and systems necessary for multiple ion beam irradiation are presented and validated experimentally. A calculation methodology was developed to quantify the spatial distribution, implantation depth and amount of energy-degraded and implanted light ions when using a thin foil rotating energy degrader during multi-ion beam irradiation. A dual ion implantation using 1.34 MeV Fe^+ ions and energy-degraded D^+ ions was conducted on single crystal silicon to benchmark the dosimetry used for multi-ion beam irradiations. Secondary Ion Mass Spectroscopy (SIMS) analysis showed good agreement with calculations of the peak implantation depth and the total amount of iron and deuterium implanted. The results establish the capability to quantify the ion fluence from both heavy ion beams and energy-degraded light ion beams for the purpose of using multi-ion beam irradiations to emulate reactor irradiated microstructures.

© 2017 Elsevier B.V. All rights reserved.

1. Introduction

Ion irradiation experiments using light and heavy ion beams have been used for decades to explore radiation damage processes. Only recently have they been applied as surrogates for reactor irradiation. Proton irradiations with damage rates of 10^{-5} dpa/s have demonstrated much success in determining the mechanistic behavior of materials under light water reactor relevant conditions [1]. Heavy ion irradiation experiments with damage rates of 10^{-3} to 10^{-4} dpa/s have replicated the microstructure observed in reactor irradiated materials also with good success [2,3]. These experiments have provided optimism for using ion irradiations as a surrogate for reactor irradiation.

Helium is known to play a role in the development of the irradiated microstructure with modifications to cavities [4–8], dislocations [9–11], and secondary phases [12–16]. Previous studies on the effects of helium using ion irradiation have used either pre-implanted or co-injected helium. The swelling behavior under ion irradiation is influenced by the mode of helium injection [17,18]. Kohyama et al. [8] used several ion irradiation schemes to assess the impact of helium injection mode on the development of cavities. Pre-injection of helium was postulated to produce a high number density of essentially immobile defects. The use of nickel ions to create a damaged microstructure followed by dual ion irradiation with nickel and helium resulted in the highest amount of swelling compared with dual ion (Ni + He) or single ion irradiation (Ni) separately. Hydrogen has been shown to modify the irradiated microstructure. Zhanbing et al. [19] irradiated a 12Cr-ODS ferritic steel to 15 dpa using dual-beam irradiation of hydrogen ions and electrons. The results showed that the dislocations were introduced at the initial stage of irradiation and were enhanced by the presence of hydrogen before developing into dislocation networks. To capture all of the effects of transmutation gas products, both helium and hydrogen need to be injected into the sample simultaneously with damage production.

The combination of helium and hydrogen together suggest a synergistic effect on the evolution of the microstructure in materials under irradiation [20–25]. The work of Wakai et al. demonstrated this synergistic effect under simultaneous displacement damage from 10.5 MeV Fe^{3+} ions with the co-injection of 1.05 MeV $He^+$and 0.38 MeV H^+in the ferritic-martensitic steel

* Corresponding author at: 2355 Bonisteel Blvd, Ann Arbor, MI 48109, USA.
E-mail address: staller@umich.edu (S. Taller).

http://dx.doi.org/10.1016/j.nimb.2017.08.035
0168-583X/© 2017 Elsevier B.V. All rights reserved.

F82H. Swelling was increased with larger cavities developing with an accompanying increase in microhardness in a ferritic-martensitic steel as compared to displacement damage combined with either helium or hydrogen co-injection alone. From these works and others [26], it is clear that multi-ion beam irradiations facilities are required to capture the synergistic behavior of gas injection and radiation damage that occurs in reactor.

Several multi-beam irradiation facilities around the world have provided significant insight into radiation damage processes, such as the facilities at TIARA [27], DuET [28], HIT [29], FZ Rossendorf [30], FSU Iena [31], LANL [32], JANNUS [33,34], the former facility at Oak Ridge National Laboratory [35] and others listed in Table 3 of reference [36]. These facilities use multiple ion accelerators in which one provides heavy ion beams to induce damage and the others to inject light ions across a range of depths in the target. A common method of controlling the light ion distribution in the target is to use multiple foils with different thicknesses on a rotating wheel [28]. A second method uses a single foil rotated in front of the beam [27]. To study the effects of simultaneous radiation damage with multiple ion beam injection, several conditions must be met and demonstrated with high fidelity. This work presents the description and validation of the systems required to perform multi-ion beam irradiation experiments for the purposes of emulating reactor environments. The major components and methodologies used at the Michigan Ion Beam Laboratory are described, including the multi-beam irradiation chamber, the irradiation stage, the thermal control systems, the dosimetry, and the thin foil energy degrader. Experiments to benchmark and validate the methods are presented as a proof-of-concept.

2. Experimental design

To allow for rigorous studies of simultaneous radiation damage and ion injection using multiple ion beams, the following conditions must be met:

i. Ion beams from multiple accelerators must be aligned so that they overlap on a single plane (the target surface).
ii. The ion beams need to be uniform across the irradiated area.
iii. The temperature of the irradiated area must be monitored and controlled to minimize the variability over the duration of the experiment, as quantified by the 2σ variation in temperature.
iv. The measurement of the total ion fluence for each species must be accurate.

2.1. Accelerators and laboratory layout

The Michigan Ion Beam Laboratory includes three accelerators: a 3 MV NEC Pelletron accelerator, a 1.7 MV General Ionex Tandem accelerator, and a 400 kV NEC Ion Implanter shown in Fig. 1. The 3 MV NEC Pelletron is a tandem accelerator used primarily for ion irradiations. The accelerator is equipped with a Peabody PS120 sputter source to generate negative ions from solid targets through sputtering and a high brightness Toroidal Volume Ion Source (TORVIS) capable of producing hydrogen and deuterium ions. The 1.7 MV General Ionex Tandem accelerator has both an Electron Cyclotron Resonance (ECR) ion source for production of positive ions with any gas, and a Multi-Cathode Source of Negative Ions by Cesium Sputtering (MC-SNICS). The 400 kV NEC Ion Implanter is a single ended accelerator where positive ions formed in the Danfysik 921A ion source are passed through a 90° bending magnet before acceleration in the accelerator tube. The ion source can operate in three modes: gas mode with a direct gas feed, liquid mode with ions produces through the vaporization of volatile compounds in a separate oven, or sputtering mode with ions produced from a solid target with argon ions. The accelerators are housed in the accelerator room and the beamlines pass through a 1.2 m thick wall into the target room that houses multiple end stations.

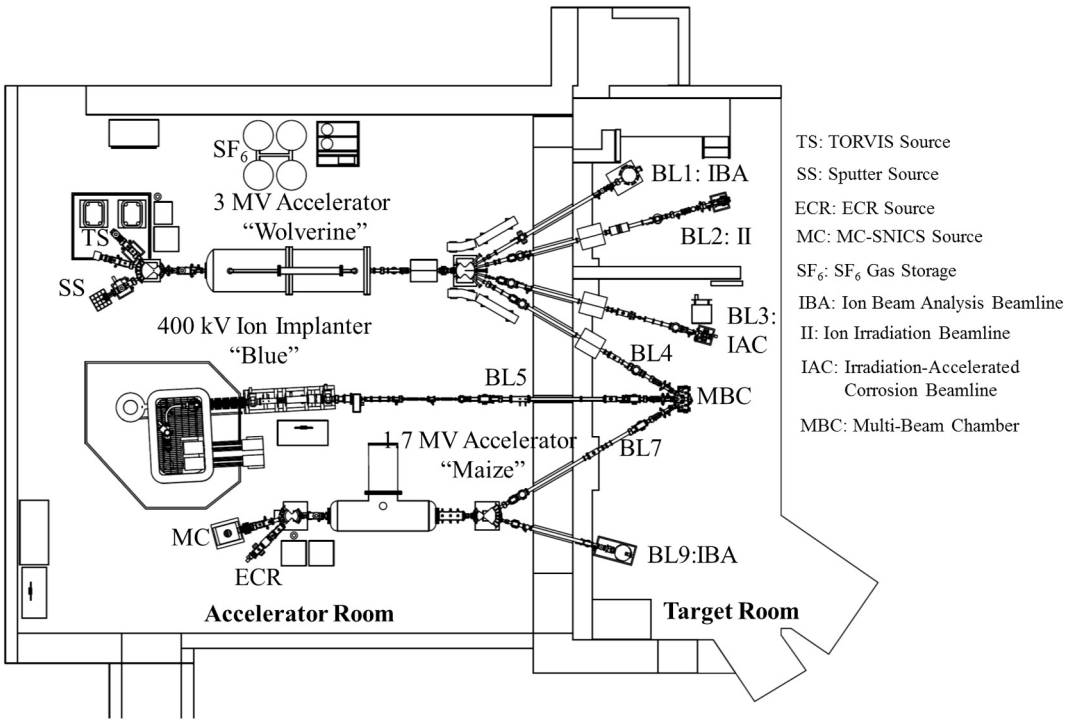


Fig. 1. The 3 MV NEC Pelletron accelerator "Wolverine", 1.7 MV General Ionex Tandem accelerator "Maize", and 400 kV NEC Ion Implanter "Blue" in the Michigan Ion Beam Laboratory.

2.2. Multi-beam chamber

The multi-beam chamber was designed to provide a fixed intersection point for each of the three accelerators. A custom-built half-cylinder shape was chosen for the chamber to provide radially directed ports, allowing direct access to the irradiation stage for the accelerators and monitoring equipment, and a flat back panel for easy access while minimizing the chamber volume, which is necessary for high vacuum. The chamber pressure, measured using calibrated vacuum ion gauges, is maintained at less than 1.33×10^{-5} Pa and baked periodically at 250 °C to ensure the high quality of the vacuum chamber. The vacuum environment is monitored using ion gauges and a residual gas analyzer. The cleanliness of the vacuum is sustained using plasma radical cleaning prior to irradiation and the use of a liquid nitrogen cooled cold trap during irradiation. The combined use of these two measures has been shown to eliminate the uptake of carbon contamination during ion irradiation [37]. Two back panels were made for the multi-beam chamber each with a 6" Conflat Flange (CF) for the irradiation stage. The angle of the 6" CF is different between the two panels to provide the stage at either 0° to face Beamline 5 (BL5) or 30° to face either Beamline 4 (BL4) or Beamline 7 (BL7).

Multi-ion beam irradiations are conducted with the stage facing Beamline 4 (BL4). BL4 delivers an ion beam from the 3 MV Pelletron accelerator, typically heavy ions for multi-beam irradiations and is normal to the ion irradiation stage. BL5 delivers a light ion beam from the 400 kV NEC Ion Implanter and is +30° from BL4 and in the same horizontal plane as BL4. BL7 delivers a light ion beam from the 1.7 MV General Ionex Tandem Accelerator for multi-beam irradiations and is +60° from BL4. This beamline may also be used for single ion beam experiments using light or heavy ions. The chamber contains ports for an ion gauge, optical camera (20° below the horizontal plane), thermal imager (−30° from the stage surface normal in the plane of the ion beams), a residual gas analyzer and many auxiliary ports for future expansion of monitoring capability of the irradiation stage.

All three accelerators are connected to the multi-beam chamber through the beamlines described previously (BL4, BL5, and BL7) and illustrated in Fig. 2. A laser is used to align each beamline between the bending magnet and the target chamber. A critical step in achieving and maintaining alignment is to minimize the use of any steering elements between the bending magnet and the target. This ensures that the beam and laser are co-linear and on the same axis down the beamline. To confirm the alignment of the multi-beam chamber at the focal point of the ion irradiation beamlines, photos showing the overlap of the laser and an ion beam were taken on a piece of alumina because it fluoresces when struck with ion beams. The alumina was marked with a grid of 2 mm × 2 mm spacing and loaded onto the irradiation stage in the position expected to be the center cross point of the three beamlines in the multi-beam chamber. The fluorescence varies in intensity with the energy and the fluence of the ion beam. Therefore, the gridded alumina piece was used to determine the location of the ion beam, but could not determine the intensity of the ion beam at any given location. An Fe^{2+} beam was used to verify the alignment of BL4 and a D^+ beam for the alignment of BL7, as shown in Fig. 3. The two ion beams are shown together in Fig. 4. The overlap of these ion beams demonstrates the capability of overlapping ion beams from multiple accelerators onto a single, well-defined area on the irradiation stage.

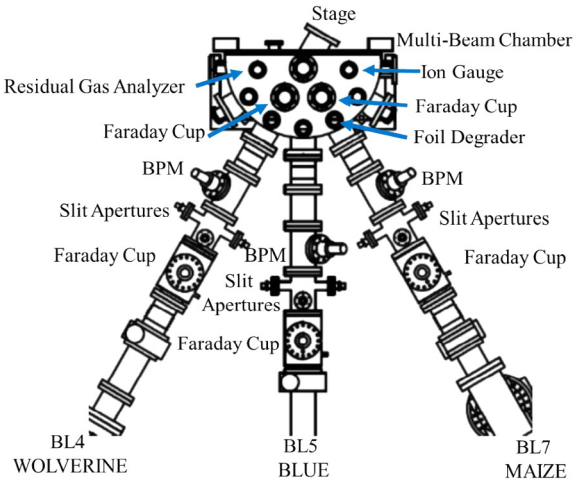


Fig. 2. Multi-beam chamber with connecting beamlines. Each beamline is equipped with Faraday cups to record the ion beam current, slit apertures to define the irradiation area, and a beam profile monitor (BPM) to assess the beam shape.

2.3. Beam intensity and profile measurement

Each beamline connected to the multi-beam chamber contains diagnostic instruments to assess the ion flux intensity and spatial profile. Suppressed Faraday cups in the beamline and the multi-beam chamber provide a measurement of beam current along each beamline with the closest Faraday cup located 12.7 cm from the sample surface. Programmable and motorized slit systems units define the irradiation area for each beamline. A beam profile monitor (BPM) located 52.0 cm from the sample surface provides a qualitative assessment of the shape of the ion beam from the slit apertures which are located 65.4 cm from the sample surface (see Fig. 2). Using the combination of Faraday cup, slit aperture, and BPM, the spatial ion flux can be quantitatively characterized within the multi-beam chamber.

Ion beams for irradiation experiments are delivered to the ion beam chamber in either raster scanned or defocused modes to provide a uniform profile across the irradiation area. To determine the ion flux distribution, a differential slit method was developed to map the spatial ion flux as illustrated schematically in Fig. 5. A Faraday cup positioned downstream from the slit aperture is used to measure the ion beam current through the slits. The slits on the aperture are then moved in 0.5 mm steps and the current in the Faraday cup is recorded (Fig. 5a). By moving each slit individually the difference in the current measured between two movements and the distance between these movements creates a measure of the current density in that small area of movement. This measurement process is conducted in both the horizontal and vertical directions to assess the spatial distribution of the ion beam at the slit aperture opening. The qualitative shape of the ion beam in the BPM and the shape from the differential slit method of profiling are compared to ensure a flat beam profile on target (Fig. 5b and c), fulfilling the need to have the beam uniformly distributed across a target area. Typical defocused ion beam profiles allow for 10% variation in current uniformity across a nominal irradiation area of up to 8 mm horizontally and 6 mm vertically.

2.4. Irradiation stage and temperature measurement

The ion irradiation stage consists of a thermally conductive copper or nickel head attached to a stainless steel tube welded onto a 6" CF flange for use with the high vacuum system. During an experiment, the stage temperature is maintained through a combination of heating from a resistive element in the metal alloy head and cooling with compressed air through channels machined into the stage head as shown in Fig. 6 similar to previous used designs [38–40]. The length of the stage was machined to match the inter-

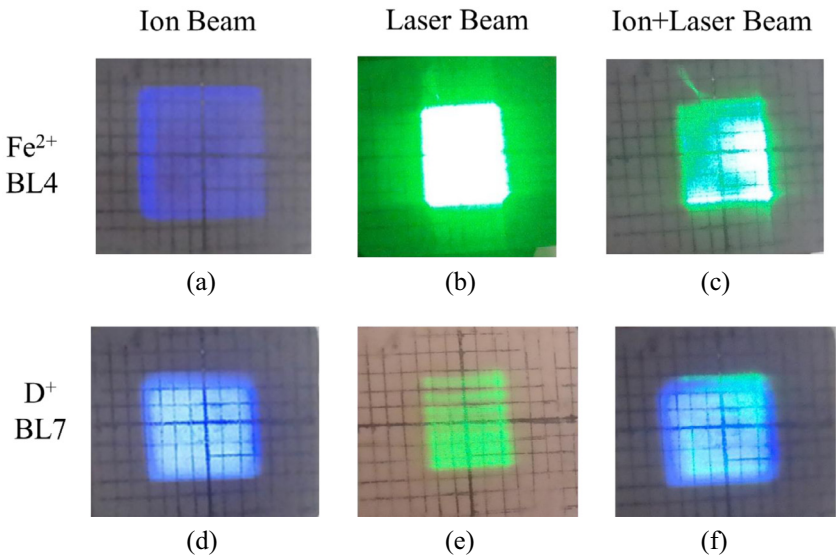


Fig. 3. Alignment of the multi-beam chamber at the multi-beam focal point with photos of an Fe^{2+} ion beam (a), laser (b), and overlapping laser and Fe^{2+} ion beam (c) from BL4 and a D^+ ion beam (d), laser (e), and overlapping laser and D^+ beam (f) from BL7 on a piece of alumina with a 2 mm × 2 mm grid.

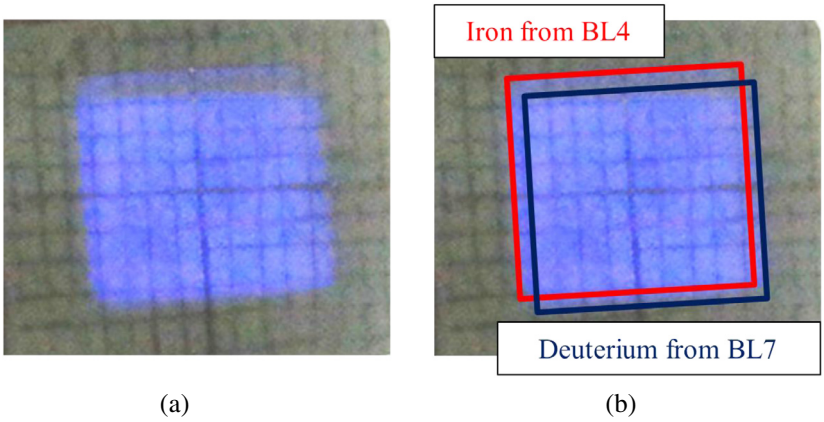


Fig. 4. Demonstration of the alignments of BL4 and BL7 into the multi-beam chamber at the multi-beam focal point by overlapping iron ion and deuterium ion beams on a marked piece of alumina (a) highlighting the individual beams (b).

section point of ion beams from BL4, BL5, and BL7 in the multi-beam chamber.

Specimens mount onto the copper stage head and are held down with a notched plate and bar for a typical multi-beam ion irradiation (Fig. 7). The notches are 1 mm in width and spaced 1 mm apart to aid in the alignment of the samples to the multi-beam intersection point. Type J thermocouples are spot-welded to samples placed just outside of the irradiation area. These thermocouples are used to calibrate a 2D infrared thermal pyrometer viewing the irradiation stage through a Ge window. The pyrometer records surface temperatures on user-defined regions of interest on the specimens at a rate of 3.125 Hz throughout the experiment. The thermal imager is calibrated against the thermocouple measurements before application of the beam for user-defined areas of interest (AOI) by adjusting the emissivity of each AOI until agreement is reached.

Before performing irradiations, the stability of the stage temperature was verified. Several samples of an austenitic steel 800H were loaded into the multi-beam chamber, prepared as if they were to be used in a multi-beam irradiation (Fig. 8a). Samples were mechanically polished and then electropolished to achieve thermal emissivity values consistent with typical samples prepared for irradiation experiments. After pumping to a pressure below 1.33×10^{-5} Pa, the samples were heated to 470 °C and held there for 20 h and continuously monitored using Type J thermocouples attached to the sample surface and the thermal imager (infrared pyrometer). The temperatures measured during this thermal stability test are shown in Fig. 8b and c for the thermocouples and a FLIR® thermal imager, respectively. The average temperatures ($T_{avg} \pm 2\sigma$) were 470.1 °C ± 2.5 °C and 470.5 °C ± 3.6 °C from thermocouples and thermal imager, respectively, for 20 h of continuous monitoring. The agreement of these two measurements demonstrates that the temperature can be maintained for an extended period of time. This temperature control and accuracy test satisfied the condition that the average temperature of the samples must be maintained with good temperature control and monitoring, demonstrated here with a 2σ variation in temperature of less than 5 °C.

3. Thin foil energy degrader

The final component used in multi-beam irradiation experiments is the thin foil energy degrader, necessary to control the

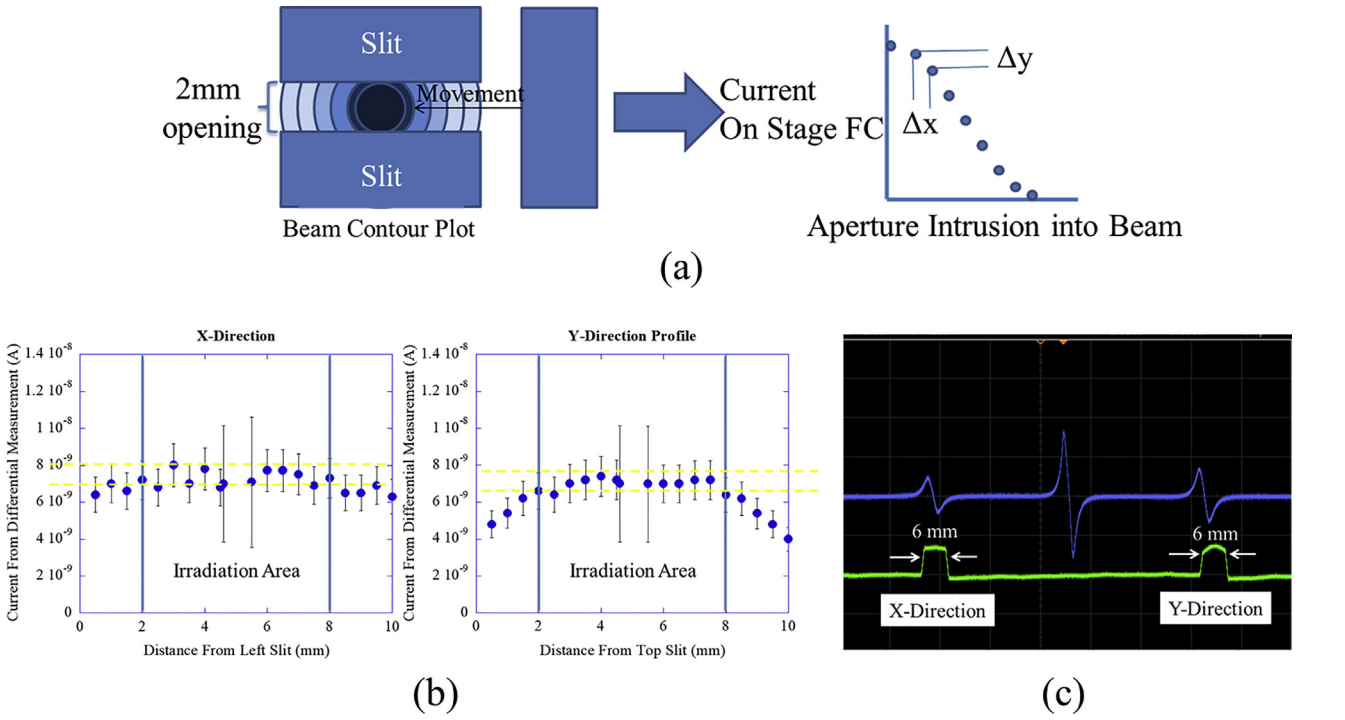


Fig. 5. a) A schematic of the differential slit method for characterization of beam uniformity, b) measured beam profiles using aperture steps across the beam with acceptable bounds of uniformity displayed as dashed yellow lines, and c) BPM profiles measured using a digital oscilloscope.

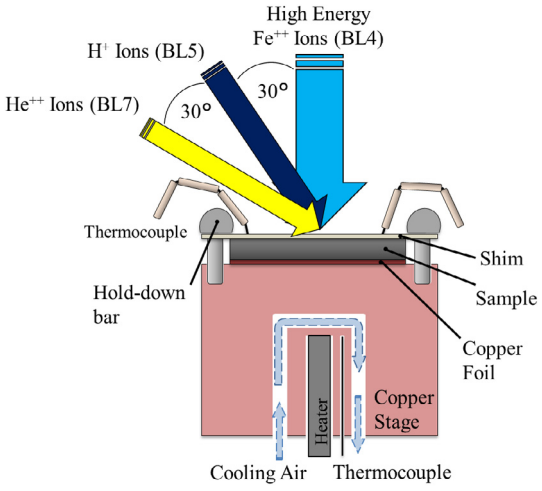


Fig. 6. Schematic drawing of the stage used for multi-ion irradiations with the stage facing BL4. The irradiation stage can also face either BL5 or BL7 to have any beam perpendicular to the samples.

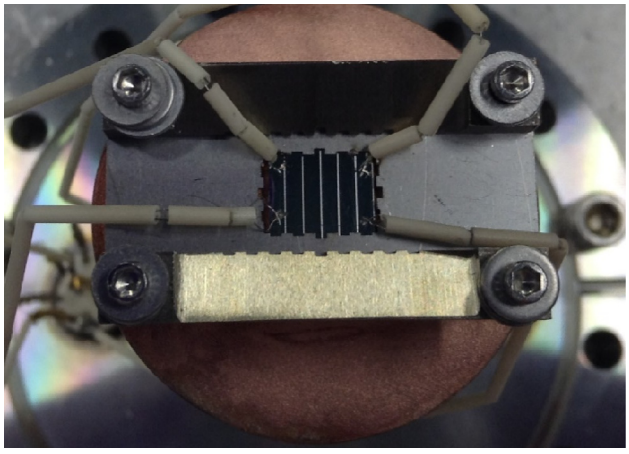


Fig. 7. An assembled multi-beam irradiation stage prior to irradiation. The notched plate and bar allow for careful alignment of the bar samples to the center of the stage and to the intersection of the multiple ion beams.

beam energy below the minimum stable voltages of the accelerators. The foil is rotatable to increase the electronic energy loss and scattering of the beam by changing the path length of the beam through the foil. By controlling the time spent at each angle during rotation, the depth of implantation can be manipulated to form any concentration profile of interest to the user. The holder consists of a stainless steel frame that secures a thin foil using a crimp, shown in Fig. 9 containing a 3 μm thick Al foil. The holder was attached to a rotatable feedthrough and controlled with a programmable stepper motor capable of rotating in 0.01° degree increments. A custom program was developed to control the rotation of the foil from 0° to 60° degrees of rotation in both clockwise and counterclockwise directions.

As the foil is rotated to increase electronic loss, the spatial flux profile also changes. To assess the ion flux as a function of both position and energy, a simple calculation method was developed using Stopping and Range of Ions in Matter (SRIM-2013) [41]. Ions enter a foil of known thickness with known ion energy, E_0, and at a foil angle of θ_0. An assumption is made that the ions are perfectly focused going into the foil as a standard input to SRIM. SRIM was then run to provide distributions in energy, position, and direction of the ions exiting the foil using the Transmit.txt output file. One hundred thousand ions were used as an input to provide a large sample size for the resulting distributions.

To develop accurate spatial distributions of ions using SRIM, the thickness of the thin foil must be known. The foil thickness was measured using several methods: direct measurement with a micrometer, Rutherford Backscattering (RBS) of the foil placed on

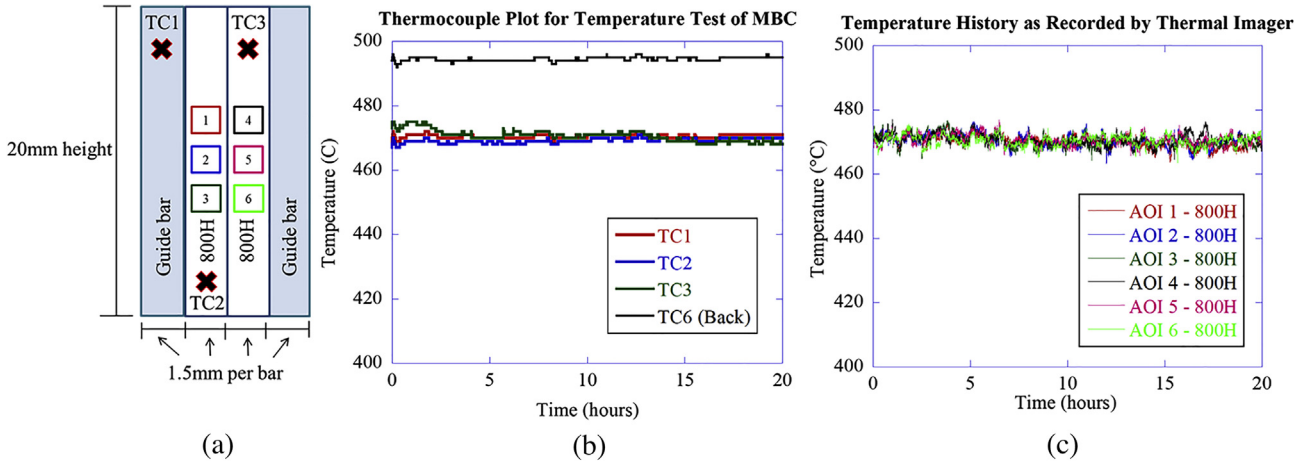


Fig. 8. A demonstration of the thermal control enforced on a multi-beam irradiation stage diagramed in (a) with locations of thermocouples (TC) and thermal imager areas AOIs compared with temperatures recorded by Type J thermocouples (b), and (c) by the FLIR® thermal imager.



Fig. 9. The thin foil energy degrader used at the Michigan Ion Beam Laboratory for control of the implantation range of a light ion beam during multi-ion irradiation through foil rotation. The holder is shown with a 2.6 μm aluminum foil loaded and held taut by a crimp inside the holder frame.

a carbon substrate, and by measuring the transmission of the ion beam current through the thin foil. To demonstrate these measurements, aluminum foils of 99.0%+ purity and varying thicknesses obtained from Goodfellow Inc. were used for all the experiments described in this work. RBS was used with a 988 keV proton beam with a detector at 160° to calculate the thickness of the aluminum foil using SimNRA [42] to match the front and back edges of the aluminum signal. The transmission through the foil was measured by taking the ratio of current in a suppressed Faraday cup before the foil and a suppressed Faraday cup after the foil in the multi-beam chamber for a deuterium ion beam in an energy range from 600 keV to 900 keV in 20 keV increments. The calculated transmission profile was estimated using SRIM to determine the ratio of ions expected at the Faraday cup. Thickness measurements using three different techniques were in good agreement; 2.4 ± 0.5 μm by micrometer, 2.6 ± 0.1 μm using transmission of the ion beam, and 2.58 ± 0.02 μm by RBS, Fig. 10.

Using the measured thickness of the aluminum foil, SRIM was used to calculate the energy, E, position vector in three dimensions, $\boldsymbol{r}$, and direction vector, $\boldsymbol{\varphi}$, in three dimensions for each ion exiting the foil and for each angle of foil rotation, $\boldsymbol{\theta}$, in one degree increments. Individual ions were then propagated from the foil to the sample surface following the direction vectors calculated with SRIM without any additional forces to alter the beam trajectory (Fig. 11). This resulted in a "plume" of ions forming a curved distribution. To ensure an even distribution of ions across the sample surface, the effects of raster scanning the beam were considered. The plume of ions was copied and added to itself with a small change (0.5 mm) in the raster scanned direction. This process was repeated until the entire raster scanned distance along the x and y directions of scanning were covered. The same variation in position would be used for a defocused ion beam passing through the foil and would be used for this simulation. The position and direction of each ion were then rotated to match the geometry between the ion beam's original direction and the irradiation stage. For this multi-beam setup, the light ion beams impinge on the sample surface at 30° and 60° to the normal of the stage surface. SRIM was used after this geometric adjustment to calculate the implantation distribution of the energy degraded ions for each angle of foil rotation. Although the foil can rotate to higher angles beyond 60°, the increased amount of scattering from the apparent thickness significantly reduces the ion beam current density at the irradiation stage and makes these angles impractical for multi-ion beam irradiations.

By measuring the position of the ions in the plane normal to the beam direction, the position and directional components of the calculations were assessed. To assess the position and direction experimentally, a 3 MeV He^{++} ion beam focused to a Full Width Half Maximum (FWHM) of 2 mm was passed through a 2.6 μm thick aluminum foil oriented perpendicular to the ion beam. An experimental setup consisting of a 1 mm diameter miniature suppressed Faraday cup faced the ion beam at 26 cm from the foil. The current was measured along x and y directions in 1 mm increments over a 25 mm travel distance in each direction to obtain the flux distribution. The experimental and computational beam intensity profiles are shown in Fig. 12a. The overall shapes are in excellent agreement. The relative intensity to the center peak was calculated to provide a comparison point between the ion beam current measured experimentally, and the number of ions used computationally in the SRIM based method described previ-

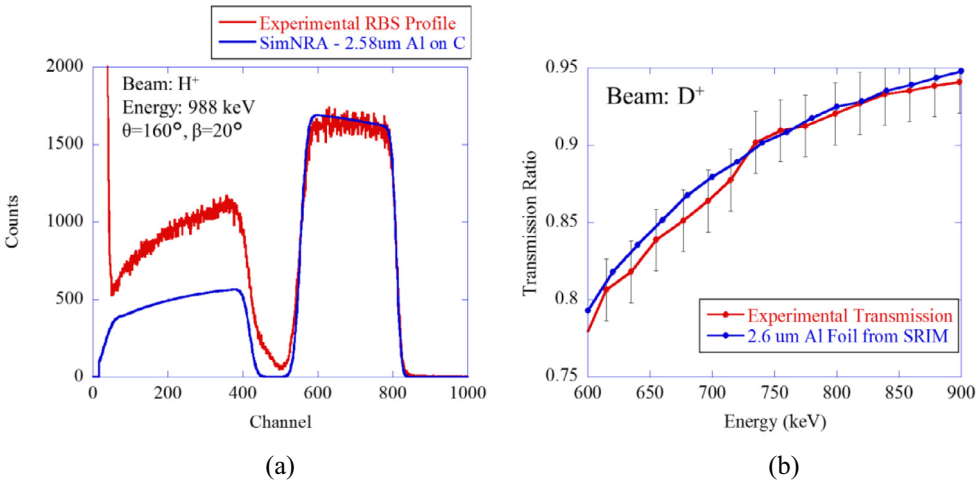


Fig. 10. Comparison between thin foil thicknesses measured with RBS (a) and transmission of an ion beam (b). As the foil thickness controls the amount of energy loss and scattering, the thickness measurement is done with multiple techniques to determine the thickness within ± 0.1 μm.

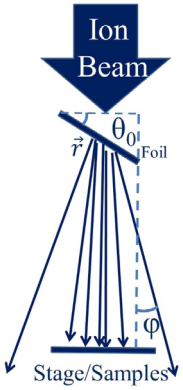


Fig. 11. A schematic of the foil degrader geometry considered for SRIM based calculations based on the foil rotation angle, θ, position of the ions after degradation, $\boldsymbol{r}$, and direction of ions from the original direction, φ.

ously. The experimental profile was found to be wider than the computational profile, but this is expected. The experimental profile was derived from a 2 mm FWHM beam and the computational profile assumed a perfect line of ions. The difference in FWHM between the profiles was approximately 2 mm, likely resulting from this assumption.

Although the rotation of the foil is used primarily to control the energy loss of the ions, the relative amount of scattering in the foil must also be measured as a function of rotation angle to quantify effects of rotation on the beam current. Using a 3.0 MeV He^{++} ion beam in both focused (2 mm FWHM) and raster-scanned conditions, the intensity of the ion beam relative to the focused beam was measured and compared to the computed intensity expected using SRIM. As shown in Fig. 12b, for both beam conditions, the peak intensities were in good agreement with foil rotation. From the measurement of the shape of the profile (Fig. 12a) and the relative intensity loss during rotation (Fig. 12b), the results from SRIM were found to adequately assess the direction, position and intensity of a thin foil degraded light ion beam. Because of the reduction in beam intensity with increasing rotation angle, achieving a uniform implantation profile requires the foil to be held for a longer time at the higher rotation angles. Between 0° and 30°, the loss in beam intensity from scattering is not significant and each angle can be rotated through quickly. For degrader angles greater than 30°, the time required to the same implanted ion concentration

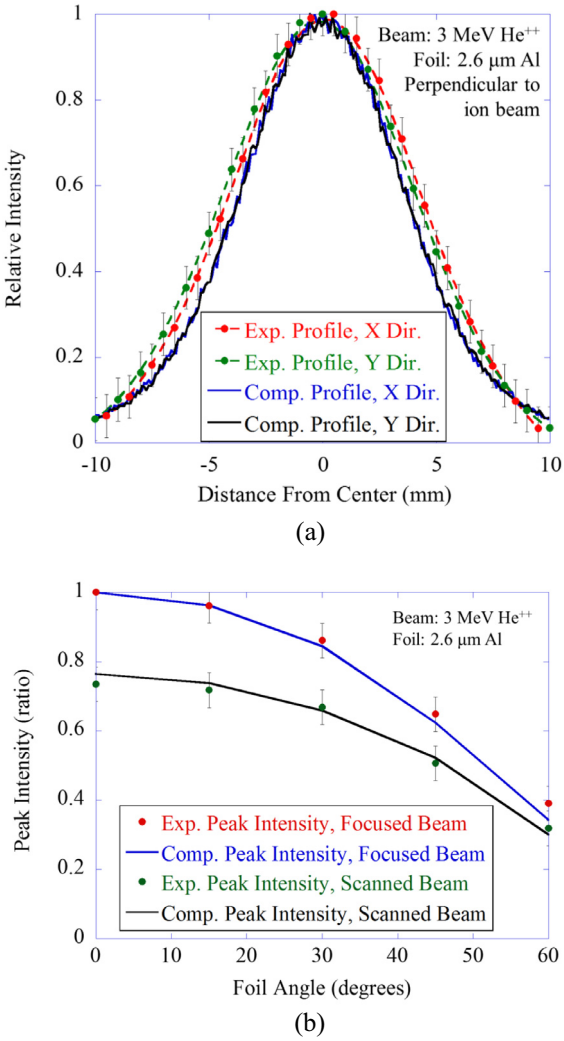


Fig. 12. Comparison between experimental and computational beam profiles for a foil held perpendicular to a light ion beam (a) showing excellent agreement in the shape of the helium ion beam after passing through a thin aluminum foil. When the foil is rotated, the computed intensity matches well with the experimental intensity for both focused and raster scanned beam conditions (b).

Table 1
Depth of peak concentration and amount of implanted species from SIMS.

Quantity	Expected	Measured
Fe concentration at peak (appm)	697	500 ± 25
Depth of Fe peak (μm)	1.22	1.21 ± 0.06
Fe fluence (10^{15} ions-cm^{-2})	1.94	1.90 ± 0.11
D concentration at peak (appm)	22	13 ± 1.5
Depth of D peak (nm)	600	585 ± 29
D fluence (10^{13} ions-cm^{-2})	4.60	4.41 ± 0.26

at each angle increases, for example for a hold time of 1 s at 30°, the hold times at 45°, 53°, 56°, and 60° are 30 s, 140 s, 150 s, and 500 s. respectively. However, Faraday cup measurements and profiling could not include an assessment of the energy of the degraded light ions.

4. Quantitative benchmarking of the multi-beam ion irradiation experimental setup

To assess the energy loss and accuracy of the implantation calculations in SRIM, energy degraded light ions were implanted into a sample with the concentration depth profile measured and compared to SRIM. This will be discussed in the following section on the quantitative benchmark of the multi-beam ion irradiation fluences using iron and deuterium ion beams. Accurate dosimetry is critical to quantifying the amount of radiation damage from the heavy ion beam and number of implanted ions from degraded light ion beams. For the heavy ion beam from BL4, the irradiation area defined by the slit aperture and periodic insertion of a large Faraday cup in front of the specimens provides the data to measure the flux of ions on the sample. Summing the ion flux over time in a piecewise constant manner provide a measurement of the total ion fluence. For an energy degraded ion beam from BL5 or BL7, the amount of scattering from the foil degrader makes a Faraday cup measurement insufficient to quantify the dose at the target area without accounting for the distance between the Faraday cup and the target area. To determine the ion flux at the irradiation stage, the scattering and intensity measurements from the calculation method described previously are used to determine the ratio of the number of ions measured at the Faraday cup to the number of ions impacting a specified area on the irradiation stage. The current in the Faraday cup is recorded during irradiation and modified using this ratio to determine the ion beam flux on the irradiated area.

To confirm our dosimetry methodology for the multi-ion beam experiments, a dual ion implantation was performed at room temperature and analyzed post-irradiation using Secondary Ion Mass Spectroscopy (SIMS). A 1.34 MeV Fe^+ beam was defocused such that the beam intensity in the irradiation area varied by less than 10% across a 5 mm × 5 mm area on a Si wafer. The beam energy was chosen to implant the peak concentration of iron at 1200 nm depth into the silicon, which is similar to the expected depth for 5 MeV iron ions implanted into steels. Measurement of the iron ion fluence was determined using a slit aperture to define the implantation area and periodic insertions of a Faraday cup to measure the ion beam current. Simultaneously, a 940 keV deuterium ion beam was raster scanned over a 9.8 μm Al foil held perpendicular to the ion beam direction to have the deuterium uniformly implanted across the irradiation area. Deuterium was chosen for its ease of detection in post-irradiation examination via secondary ion mass spectroscopy (SIMS). The estimated fluence was determined using the SRIM-based calculation method described previously.

The resulting implanted silicon wafer was analyzed using Dynamic Secondary Ion Mass Spectroscopy (D-SIMS) at Surface Science Western at the University of Western Ontario using a Cameca® IMS-3f SIMS. An oxygen primary beam was used to profile the iron while monitoring positive ions, and a cesium primary beam was used to profile the deuterium while monitoring negative ions. The depth scale was calibrated by measuring the depth of the SIMS craters with a KLA Tencor P-10 Surface Profiler. The results were compared to the expected depth profiles and ion fluences from SRIM. The results from this analysis are shown in Table 1 and Fig. 13. The peak of the implanted iron was expected to be 1.22 μm into the silicon, and the measurement yielded a peak at 1.21 ± 0.06 μm. The peak of the deuterium concentration was predicted to be about 600 nm into the material and measured to be at about 585 ± 29 nm. The agreement between the SRIM calculated and measured depths provides confidence in SRIM for the location of implanted ions whether directly from the accelerator (iron beam normal to the target) or after energy degradation (deuterium beam at 60° to normal). The peak implanted concentrations for the iron and deuterium are both lower than the SRIM predicted values. However, when the concentration profiles are integrated, the measured fluences from SIMS were within 10% of the expected values (Table 1). The excellent agreement of these fluence values provides confidence that the dosimetry measurements taken during multi-beam ion irradiations are accurate, fulfilling the last requirement to performing successful, well-controlled multi-beam ion irradiations.

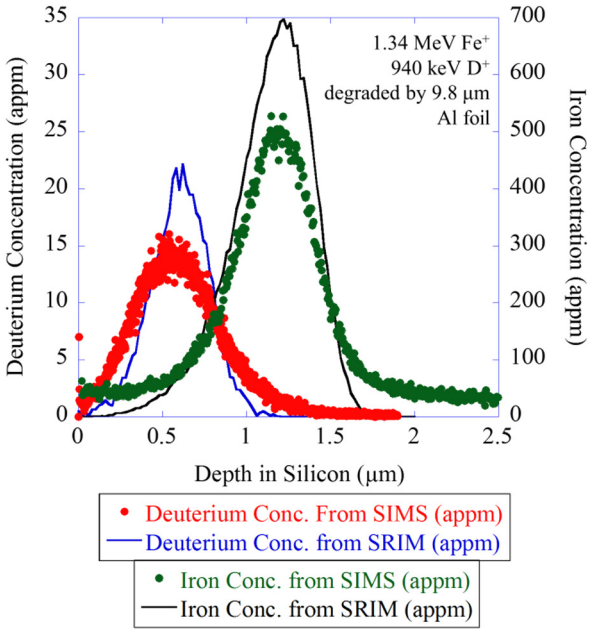


Fig. 13. Concentration of Fe and D with depth in Si wafer measured with dynamic SIMS and calculated using SRIM 2013.

Having demonstrated the capability to perform multi-beam ion irradiations, the removal of surface material through sputtering is a concern because of the shallow ion range and geometry of the setup. In the configuration used for multiple ion beam irradiations, the heavy ion beam impacts the sample normal to the surface to maximize the ion range. Using SRIM as an estimation of 5 MeV Fe ions hitting an iron target (E_d = 40 eV, E_{surf} = 4.34 eV) in the Monolayer/Surface Sputtering calculation mode, the sputtering yield varied from 0.94 to 1.03 atoms/ion for a run of 50,000 ions. For multiple ion beam irradiations, the helium (60° to the target surface) and hydrogen (30° to the target surface) are implanted in a range from 300 nm to 1000 nm. Again, estimating the sputtering with SRIM for the maximum and minimum light ion energy for this ion range and geometry, the sputtering yield was 0.01–

0.05 atoms/ion for helium, and 0.001–0.003 atoms/ion for hydrogen. This calculation is sensitive to the input surface binding energy. Changes to the surface binding energy from surface roughness and surface stoichiometry for alloys were not considered. Based on the relative values of the sputtering yield for each specie, the additional sputtering from the light ion beams can be considered negligible until reaching the hundreds to thousands of appm gas/dpa ratio where the fluxes of the light ion species become orders of magnitude larger than the flux of heavy ions. A recent paper [43] considered the effects of sputtering from 5 MeV iron ions up to a fluence of 1×10^{18} ions/cm^2, (nominally 400 dpa at an examination depth of 600 nm in iron). These results suggest that the displacement damage and ion implantation curves are not significantly modified up to 400 dpa from the heavy ion irradiations. Combining this interpretation with the SRIM calculations previously presented, sputtering will not be a significant concern in multiple ion beam irradiations until high doses are achieved or when irradiated with high gas/dpa ratios.

A distinguishing feature of multi-beam irradiations conducted in the Michigan Ion Beam Laboratory is the capability to control components remotely through an internet protocol network. This enables all instruments in the laboratory (ion sources, accelerators, beamline components, and target chamber instrumentation) to be monitored and controlled remotely from the Control Room or from any computer on the lab network. Each accelerator has a single control computer for its set of components from ion source to target. After loading a set of samples onto the irradiation stage and pumping down the chamber, the remainder of the setup and execution of the irradiation experiment is controlled remotely. The liquid nitrogen cold trap maintains temperature using sensors to measure the remaining liquid in the dewar and refill automatically once the liquid reaches a set level. The heater and air cooling are controlled with a user interface with simultaneous read-back of the thermocouples and the thermal camera. Steering, focusing and alignment of the ion beams are verified using a marked grid of alumina. Analog signals from each device, such as the magnets, electrostatic steerers, and Faraday cups are digitized using embedded hardware. The digitization of the signals also allows selected signals to be logged in a database for recall or displayed in real time, ensuring the quality of multiple ion beam irradiations.

Multiple ion beam facilities worldwide are divided into three categories as defined in [36,44]: those with multiple accelerators and implanters, those in which a transmission electron microscope (TEM) is coupled with accelerators, and those in which the TEM is coupled with an ion gun source. The recent renovation of the Michigan Ion Beam Laboratory falls into the first category, and the laboratory will soon join the latter two categories. The capability to perform multiple ion beam irradiations from three accelerators in a well-monitored and tightly controlled manner creates new opportunities to explore radiation damage phenomena. The Michigan Ion Beam Laboratory will be used to investigate the effects of the gas/dpa ratio, temperature (cryogenic to 1200 °C), damage (up to hundreds of dpa) and damage rate (10^{-5} to 10^{-3} dpa/s) on the evolution of irradiated microstructures up to high damage levels. These experiments will be used to assess the behavior of materials at reactor relevant conditions to provide guidance on using ion irradiations as a surrogate for reaction irradiation.

5. Summary

To study the effects of simultaneous radiation damage with multiple ion beam injection, several conditions must be met. First, ion beams from multiple accelerators must overlap on a single plane at the sample surface. The design and configuration of the multi-beam chamber provides for multiple ion beams to intersect, as verified by fluorescence of gridded alumina. Second, to ensure a uniform beam across the target area, each beamline used for a multiple ion beam irradiation must have the diagnostic instruments to assess the ion flux distribution in space and intensity using a combination of a beam profile monitor, slit aperture, and suppressed Faraday cup. Third, the average temperature of the irradiation area must be maintained with good temperature control and monitoring, as quantified by the 2σ variation in temperature. The stability and accuracy of the temperature control has been demonstrated using a thermal imager benchmarked against thermocouples. Experimental measurements of a light ion beam passing through a thin foil energy degrader were found to agree very well with SRIM based calculations through a thin Al foil.

Finally, the measurement of the total fluence of ions from each beam must be reliable and accurate. A dual ion implantation using a heavy ion beam (Fe^+) and an energy degraded light ion beam (D^+) was conducted on a piece of silicon at room temperature to benchmark the dosimetry. Excellent agreement between target and measurement was found for both the depth distribution of the implanted ions and the total amount of iron and deuterium implanted. These findings provide confidence in the capability to quantify the ion irradiation fluence from both heavy ion beams and energy degraded light ion beams for multi-ion beam irradiations.

Acknowledgements

The authors gratefully acknowledge the support provided by DOE – Nuclear Energy Program, the Electric Power Research Institute (EPRI), TerraPower Inc. through the research roundtable agreement DRDA 11-PAF05786, Oak Ridge National Laboratory, the University of Michigan College of Engineering, and the University of Michigan Nuclear Engineering and Radiological Sciences (NERS) department for the renovation of the Michigan Ion Beam Laboratory. Parts of this work supported by DOE NEUP IRP under award DE-NE0000639. This material is based upon research supported under a DOE NEUP Graduate Fellowship. The authors also acknowledge the staff at Surface Science Western for their discussions.

References

[1] K.J. Stephenson, G.S. Was, Comparison of the microstructure, deformation and crack initiation behavior of austenitic stainless steel irradiated in-reactor or with protons, J. Nucl. Mater. 456 (2015) 85–98, http://dx.doi.org/10.1016/j.jnucmat.2014.08.021.
[2] G.S. Was, Z. Jiao, E. Getto, K. Sun, A.M. Monterrosa, S.A. Maloy, O. Anderoglu, B. H. Sencer, M. Hackett, Emulation of reactor irradiation damage using ion beams, Scr. Mater. 88 (2014) 33–36, http://dx.doi.org/10.1016/j.scriptamat.2014.06.003.
[3] E. Getto, Z. Jiao, A.M. Monterrosa, K. Sun, G.S. Was, Effect of pre-implanted helium on void swelling evolution in self-ion irradiated HT9, J. Nucl. Mater. 462 (2015) 458–469, http://dx.doi.org/10.1016/j.jnucmat.2015.01.045.
[4] P.J. Maziasz, R.L. Klueh, J.M. Vitek, Helium effects on void formation in 9Cr-1MoVNb and 12Cr-1MoVW irradiated in HFIR, J. Nucl. Mater. 141–143 (1986) 929–9337, http://dx.doi.org/10.2172/5124729.
[5] D.S. Gelles, A. Kohyama, Microstructural Examination of HT-9 in the FFTF/MOTA to 110 dpa, in: Fusion React. Mater. Semiannu. Prog. Rep. Period End. March 31, 1989, Department of Energy DOE/ER-031316, Oak Ridge, TN, 1989: p. 193.
[6] C.Y. Hsu, D.S. Gelles, T.A. Lechtenberg, Microstructural Examination of 12% Cr Martensitic Stainless Steel After Irradiation at Elevated Temperatures in FFTF, in: F.A. Garner, N.H. Packan, A.S. Kumar (Eds.), Radiation-Induced Chang. Microstruct. ASTM STP 955, American Society for Testing and Materials, Philadelphia, PA, 1987: p. 545.
[7] K. Asano, Y. Kohno, A. Kohyama, G. Ayrault, Microstructural evolution of HT9 under dual-beam charged particle irradiation, J. Nucl. Mater. 157 (1988) 912–915.
[8] A. Kohyama, G. Ayrault, N. Igata, Microstructural evolution in dual-ion irradiated 316ss under various helium injection schedules, J. Nucl. Mater. 122 (1984) 224–229, http://dx.doi.org/10.1016/0022-3115(84)90600-7.

[9] F. Wan, Q. Zhan, Y. Long, S. Yang, G. Zhang, Y. Du, Z. Jiao, S. Ohnuki, The behavior of vacancy-type dislocation loops under electron irradiation in iron, J. Nucl. Mater. 455 (2014) 253–257, http://dx.doi.org/10.1016/j.jnucmat.2014.05.048.
[10] K. Farrell, P.J. Maziasz, E.H. Lee, L.K. Mansur, Modification of radiation damage microstructure by helium, Radiat. Eff. 78 (1983) 277–295, http://dx.doi.org/10.1080/00337578308207378.
[11] H. Seto, N. Hashimoto, H. Kinoshita, S. Ohnuki, Effects of multi-beam irradiation on defect formation in Fe-Cr alloys, J. Nucl. Mater. 417 (2011) 1018–1021, http://dx.doi.org/10.1016/j.jnucmat.2011.01.053.
[12] E.A. Kenik, The influence of helium on microstructuralevolution in an ion-irradiated low-swelling stainless steel, J. Nucl. Mater. 85–86 (1979) 659–663, http://dx.doi.org/10.1016/0022-3115(79)90335-0.
[13] A.F. Rowcliffe, E.H. Lee, High temperature radiation damage phenomena in complex alloys, J. Nucl. Mater. 108–109 (1982) 306–318, http://dx.doi.org/10.1016/0022-3115(82)90500-1.
[14] A. Hishinuma, N.H. Packan, E.H. Lee, L.K. Mansur, Effects of pulsed and/or dual ion irradiation on microstructural evolution in a Ti and Si modified austenitic alloy, J. Nucl. Mater. 122 (1984) 260–265, http://dx.doi.org/10.1016/0022-3115(84)90607-X.
[15] E.H. Lee, N.H. Packan, L.K. Mansur, Effects of pulsed dual-ion irradiation on phase transformations and microstructure in Ti-modified austenitic alloy, J. Nucl. Mater. 117 (1983) 123–133, http://dx.doi.org/10.1016/0022-3115(83)90018-1.
[16] W.J. Choyke, J.N. Mcgruer, J.R. Townsend, J.A. Spitznagel, N.J. Doyle, F.J. Venskytis, Helium effects in ion-bombarded 304 stainless steel, J. Nucl. Mater. 85–86 (1979) 647–651, http://dx.doi.org/10.1016/0022-3115(79)90333-7.
[17] N.H. Packan, K. Farrell, Simulation of first wall damage: effects of the method of gas implantation, J. Nucl. Mater. 85–86 (1979) 677–681, http://dx.doi.org/10.1016/0022-3115(79)90338-6.
[18] L.K. Mansur, W.A. Coghlan, Mechanisms of helium interaction with radiation effects in metals and alloys: a review, J. Nucl. Mater. 119 (1983) 1–25, http://dx.doi.org/10.1016/0022-3115(83)90047-8.
[19] Y. Zhanbing, H. Benfu, H. Kinoshita, H. Takahashi, S. Watanabe, Effect of hydrogen ion/electron dual-beam irradiation on microstructural damage of a 12Cr-ODS ferrite steel, J. Nucl. Mater. 398 (2010) 81–86, http://dx.doi.org/10.1016/j.jnucmat.2009.10.014.
[20] E. Wakai, Y. Miwa, N. Hashimoto, J.P. Robertson, R.L. Klueh, K. Shiba, K. Abiko, S. Furuno, S. Jitsukawa, Microstructural study of irradiated isotopically tailored F82H steel, J. Nucl. Mater. 307–311 (2002) 203–211.
[21] E. Wakai, M. Ando, T. Sawai, S. Ohnuki, Effect of helium and hydrogen production on irradiation hardening of F82H steel irradiated by ion beams, Mater. Trans. 48 (2007) 1427–1430, http://dx.doi.org/10.2320/matertrans.MBW200611.
[22] E. Wakai, M. Ando, T. Sawai, K. Kikuchi, K. Furuya, M. Sato, K. Oka, S. Ohnuki, H. Tomita, T. Tomita, Y. Kato, F. Takada, Effect of gas atoms and displacement damage on mechanical properties and microstructures of F82H, J. Nucl. Mater. 356 (2006) 95–104, http://dx.doi.org/10.1016/j.jnucmat.2006.05.032.
[23] T. Tanaka, K. Oka, S. Ohnuki, S. Yamashita, T. Suda, S. Watanabe, E. Wakai, Synergistic effect of helium and hydrogen for defect evolution under multi-ion irradiation of Fe–Cr ferritic alloys, J. Nucl. Mater. 329–333 (2004) 294–298, http://dx.doi.org/10.1016/j.jnucmat.2004.04.051.
[24] E. Wakai, T. Sawai, K. Furuya, A. Naito, T. Aruga, K. Kikuchi, S. Yamashita, S. Ohnuki, S. Yamamoto, H. Naramoto, S. Jistukawa, Effect of triple ion beams in ferritic/martensitic steel on swelling behavior, J. Nucl. Mater. 307–311 (2002) 278–282.
[25] S. Hamada, Y.C. Zhang, Y. Miwa, D. Yamaki, Effect of triple beam irradiation on microstructural evolution in austenitic stainless steel, Radiat. Phys. Chem. 50 (1997) 555–559, http://dx.doi.org/10.1016/S0969-806X(97)00102-3.
[26] J. Marian, T. Hoang, M. Fluss, L.L. Hsiung, A review of helium–hydrogen synergistic effects in radiation damage observed in fusion energy steels and an interaction model to guide future understanding, J. Nucl. Mater. 462 (2015) 409–421, http://dx.doi.org/10.1016/j.jnucmat.2014.12.046.
[27] S. Hamada, Y. Miwa, D. Yamaki, Y. Katano, T. Nakazawa, K. Noda, Development of a triple beam irradiation facility, J. Nucl. Mater. 258–263 (1998) 383–387, http://dx.doi.org/10.1016/S0022-3115(98)00232-3.
[28] A. Kohyama, Y. Katoh, M. Ando, K. Jimbo, A new multiple beams-material interaction research facility for radiation damage studies in fusion materials, Fusion Eng. Des. 51–52 (2000) 789–795, http://dx.doi.org/10.1016/S0920-3796(00)00181-2.
[29] Y. Kohno, K. Asano, A. Kohyama, K. Hasegawa, N. Igata, New dual-ion irradiation station at the University of Tokyo, J. Nucl. Mater. 141–143 (1986) 794–798, http://dx.doi.org/10.1016/0022-3115(86)90095-4.
[30] J.R. Kaschny, R. Kögler, H. Tyrrof, W. Bürger, F. Eichhorn, A. Mücklich, C. Serre, W. Skorupa, Facility for simultaneous dual-beam ion implantation, Nucl. Instrum. Meth. Phys. Res. Sect. A Accel. Spectrom. Detect. Assoc. Equip. 551 (2005) 200–207, http://dx.doi.org/10.1016/j.nima.2005.06.046.
[31] B. Breeger, E. Wendler, W. Trippensee, C. Schubert, W. Wesch, Two-beam irradiation chamber for in situ ion-implantation and RBS at temperatures from 15 K to 300 K, Nucl. Instrum. Meth. Phys. Res. Sect. A Accel. Spectrom. Detect. Assoc. Equip. 174 (2001) 199–204, http://dx.doi.org/10.1016/S0168-583X(00)00433-X.
[32] N. Yu, M. Nastasi, T.E. Levine, J.R. Tesmer, M.G. Hollander, C.R. Evans, C.J. Maggiore, In-situ capability of ion beam modification and characterization of materials at Los Alamos National Laboratory, Nucl. Instrum. Meth. Phys. Res. Sect. A Accel. Spectrom. Detect. Assoc. Equip. 99 (1995) 566–568, http://dx.doi.org/10.1016/0168-583X(94)00702-0.
[33] Y. Serruys, P. Trocellier, S. Miro, E. Bordas, M.O. Ruault, O. Kaïtasov, S. Henry, O. Leseigneur, T. Bonnaillie, S. Pellegrino, S. Vaubaillon, D. Uriot, JANNUS: a multi-irradiation platform for experimental validation at the scale of the atomistic modelling, J. Nucl. Mater. 386–388 (2009) 967–970, http://dx.doi.org/10.1016/j.jnucmat.2008.12.262.
[34] P. Trocellier, Y. Serruys, S. Miro, E. Bordas, S. Pellegrino, S. Vaubaillon, M.O. Ruault, S. Henry, O. Kaitasov, Application of multi-irradiation facilities, Nucl. Instrum. Meth. Phys. Res. Sect. B-Beam Interact. Mater. Atoms. 266 (2008) 3178–3181, http://dx.doi.org/10.1016/j.nimb.2008.03.224.
[35] M.B. Lewis, W.R. Allen, R.A. Buhl, N.H. Packan, S.W. Cook, L.K. Mansur, Triple ion beam irradiation facility, Nucl. Instrum. Meth. Phys. Res. Sect. A Accel. Spectrom. Detect. Assoc. Equip. 43 (1989) 243–253, http://dx.doi.org/10.1016/0168-583X(89)90045-1.
[36] M. Fluss, W.E. King, Report on the Workshop for Science Applications of a Triple Beam Capability for Advanced Nuclear Energy Materials, Lawrence Livermore National Laboratory, LLNL-MI-413125, 2009.
[37] G.S. Was, S. Taller, Z. Jiao, A.M. Monterrosa, D. Jennings, T. Kubley, F. Naab, O. Toader, E. Uberseder, Resolution of the carbon contamination problem in ion irradiation experiments, Nucl. Instrum. Meth. Phys. Res. Sect. B-Beam Interact. Mater. Atoms (2017), Submitted.
[38] D.L. Damcott, J.M. Cookson, V.H. Rotberg, G.S. Was, A radiation effects facility using a 1.7 MV tandem accelerator, Nucl. Inst. Meth. Phys. Res. B. 99 (1995) 780–783, http://dx.doi.org/10.1016/0168-583X(94)00618-0.
[39] J.J. Penisten, The Mechanism of Radiation-Induced Segregation in Ferritic-Martensitic Steels, University of Michigan, 2012.
[40] E.M. Getto, The Co-Evolution of Microstructure Features in Self-Ion Irradiated HT9 at Very High Damage Levels, University of Michigan, 2016.
[41] J.F. Ziegler, M.D. Ziegler, J.P. Biersack, SRIM – The stopping and range of ions in matter (2010), Nucl. Instrum. Meth. Phys. Res. Sect. A Accel. Spectrom. Detect. Assoc. Equip. 268 (2010) 1818–1823, http://dx.doi.org/10.1016/j.nimb.2010.02.091.
[42] M. Mayer, SIMNRA, a simulation program for the analysis of NRA, RBS and ERDA, AIP Conf. Proc. 475 (1999) 541–544, http://dx.doi.org/10.1063/1.59188.
[43] J. Wang, M.B. Toloczko, N. Bailey, F.A. Garner, J. Gigax, L. Shao, Modification of SRIM-calculated dose and injected ion profiles due to sputtering, injected ion buildup and void swelling, Nucl. Instrum. Meth. Phys. Res. Sect. A Accel. Spectrom. Detect. Assoc. Equip. 387 (2016) 20–28, http://dx.doi.org/10.1016/j.nimb.2016.09.015.
[44] Y. Serruys, M. Ruault, P. Trocellier, S. Miro, A. Barbu, L. Boulanger, O. Kaitasov, S. Henry, O. Leseigneur, P. Trouslard, JANNUS: experimental validation at the scale of atomic modelling, Comptes Rendus Phys. 9 (2008) 437–444, http://dx.doi.org/10.1016/j.crhy.2007.10.015.